

## ORIGINAL ARTICLE

# Structural Connectivity Fingerprints Predict Cortical Selectivity for Multiple Visual Categories across Cortex

David E. Osher<sup>1,2</sup>, Rebecca R. Saxe<sup>1</sup>, Kami Koldewyn<sup>1,3</sup>, John D.E. Gabrieli<sup>1</sup>, Nancy Kanwisher<sup>1</sup>, and Zeynep M. Saygin<sup>1</sup>

<sup>1</sup>McGovern Institute for Brain Research, Massachusetts Institute of Technology, Cambridge, MA, USA,

<sup>2</sup>Department of Psychological and Brain Sciences, Boston University, Boston, MA, USA, and <sup>3</sup>School of Psychology, Bangor University, Gwynedd, UK

Address correspondence to: Dr David Osher, Department of Psychological and Brain Sciences, Boston University, 2 Cummington Mall, Rm 109, Boston, MA 02215, USA. Email: osher@bu.edu

## Abstract

A fundamental and largely unanswered question in neuroscience is whether extrinsic connectivity and function are closely related at a fine spatial grain across the human brain. Using a novel approach, we found that the anatomical connectivity of individual gray-matter voxels (determined via diffusion-weighted imaging) alone can predict functional magnetic resonance imaging (fMRI) responses to 4 visual categories (faces, objects, scenes, and bodies) in individual subjects, thus accounting for both functional differentiation across the cortex and individual variation therein. Furthermore, this approach identified the particular anatomical links between voxels that most strongly predict, and therefore plausibly define, the neural networks underlying specific functions. These results provide the strongest evidence to date for a precise and fine-grained relationship between connectivity and function in the human brain, raise the possibility that early-developing connectivity patterns may determine later functional organization, and offer a method for predicting fine-grained functional organization in populations who cannot be functionally scanned.

**Key words:** diffusion-weighted imaging, structure–function, tractography, visual perception

## Introduction

A deep-rooted assumption in neuroscience holds that a region's function is primarily determined by its extrinsic connectivity. Indeed, one of the key-defining properties of a cortical area is its pattern of connectivity to the rest of the brain, an idea supported by extensive evidence from tracer studies in macaques (Ungerleider and Mishkin 1982; Felleman and Van Essen 1991; Passingham et al. 2002; Jbabdi, Lehman, et al. 2013). However, great functional diversity exists within cortical regions, wherein neighboring neural clusters prefer different stimulus properties (Colby and Goldberg 1999; Moeller et al. 2008). Specific connectivity patterns may be necessary for functional diversity at a finer spatial grain, and recent studies have begun to explore this relationship between anatomical projections and cortical specialization

(Moeller et al. 2008; Bock et al. 2011; Briggman et al. 2011; Glickfeld et al. 2013). Yet it remains largely unknown whether connectivity predicts function at a fine grain in the human brain, particularly for nonprimary cortical regions engaged in higher cognitive functions.

The best evidence for a close relationship between extrinsic connectivity and function in the human brain comes from the combination of diffusion-weighted imaging (DWI) and functional imaging using functional magnetic resonance imaging (fMRI) (for review, see Jbabdi and Behrens 2013). Pioneering studies have shown that sharp changes in DWI connectivity occur at the boundaries of functionally defined regions that can be identified through cytoarchitectonics (e.g., Johansen-Berg et al. 2004; Saygin et al. 2011) and at the boundaries of posited functional divisions based on meta-analyses (Tomassini et al. 2007;

Beckmann et al. 2009; Mars et al. 2011, 2012, 2013; Sallet et al. 2013). However, it is unknown 1) whether connectivity patterns can also characterize high-level regions defined in an individual subject, including regions that are highly variable across individuals (Saxe et al. 2006; Fedorenko et al. 2010; Frost and Goebel 2012), and 2) whether the relationship between connectivity and function holds at a finer grain than the level of whole cortical areas. Here, we test these hypotheses by integrating DWI with fMRI and assessing the degree to which we can predict the neural response of any cortical voxel using only the connectivity pattern of that voxel.

This work bears directly on 3 important points. First, as just noted, the presence of a fine-scaled topographic relationship between extrinsic connectivity and function is a longstanding and fundamental question in neuroscience (Jbabdi, Sotiropoulos, et al. 2013), and is largely unknown for higher level functions of the human brain. Second, according to one influential hypothesis, extrinsic connections play a key role in directing brain development, instructing the functional development of cortical regions by determining the information each receives (Sur et al. 1988). If it is generally true that areal specialization arises developmentally as a consequence of pre-existing differentiation in connectivity patterns across the cortex, then we should see a tight relationship between extrinsic connectivity and function in adults (and we would further predict that differentiation of connectivity patterns across the cortex precedes differentiation of function). Third, the ability to predict the functional organization of an individual's brain from the pattern of connectivity in the same individual would have substantial clinical applications, enabling functional maps to be derived for individuals who cannot be functionally scanned because they are comatose, unable to perform the tasks required for functional scanning, or unable to lie still without sedation.

Recently, a novel approach that integrates DWI and fMRI was developed to assess the relationship between structural connectivity and functional specificity, and was tested for the fusiform gyrus in humans (Saygin et al. 2012). Specifically, we showed that the face selectivity of each voxel in the fusiform gyrus within individual subjects could be predicted from the strength of connection of that voxel to the rest of the brain (its unique connectivity profile, or fingerprint), as measured through DWI. Here, we test whether this relationship between connectivity and face selectivity is found more generally for other cortical regions and for other kinds of functional specificity.

If a tight relationship between connectivity and function is a general principle of the cortex, then we predict that we will find a similar ability to predict other visual functional selectivities across cortex. Another possibility, however, is that the connectivity–function relationship may be unique to or stronger for faces, which have great evolutionary significance to primates. Substantial evidence from behavioral, neuroimaging, electrophysiological, and lesion work indicates that faces are processed by distinct neural mechanisms specialized for faces per se (Warrington and James 1967; Desimone et al. 1984; Perrett et al. 1992; Kanwisher et al. 1997; McCarthy et al. 1997; Tsao et al. 2006; Freiwald and Tsao 2014). Some behavioral evidence even suggests that these mechanisms may develop with little or no visual experience of faces (Sugita 2008; Turati et al. 2008; Rosa-Salva et al. 2010). Thus, faces are a “special” visual category in numerous respects (McKone and Robbins 2011), so we cannot assume that the tight relationship we found between connectivity and face selectivity in fusiform cortex will generalize to other visual categories or regions.

To answer this question, we acquired both DWI and fMRI images from each subject while they viewed stimuli from multiple visual categories (faces, bodies, objects, and scenes), and

we tested whether a voxel's unique connectivity pattern can predict that voxel's functional selectivity to each of these visual categories. For each anatomically defined parcel, we trained a computational model on the voxel-wise relationship between connection probabilities and fMRI responses across subjects, and applied the resulting model to a new participant's connectivity data, which resulted in voxel-wise-predicted fMRI responses for that new participant. We compared each subject's fMRI predictions from connectivity with that subject's actual fMRI responses, and also to fMRI predictions based on fMRI maps from other subjects (i.e., group-average benchmark model). Lastly, in order to better characterize the connections that may underlie brain function, we identified the connections that most strongly predicted each visual category, and analyzed these predictive networks with graph theoretical approaches.

## Materials and Methods

### Participants

DWI and fMRI data were collected from 30 participants; of these, 4 participants were excluded from subsequent analyses due to excessive motion (determined by visual inspection). Analyses included 26 participants (mean age = 26.0, 11 M:15 F) who were recruited from the greater Boston area. Participants were screened for history of mental illness, gave written informed consent, and were compensated at \$30 per hour. The study was approved by the Massachusetts Institute of Technology and Massachusetts General Hospital ethics committees.

### DWI Acquisition Parameters and Tractography

DWI data were acquired using echo planar imaging (64 slices, voxel size  $2 \times 2 \times 2$  mm,  $128 \times 128$  base resolution, diffusion weighting isotropically distributed along 30 directions,  $b$ -value  $700 \text{ s mm}^{-2}$ ) on a 3-T Siemens scanner with a 32-channel head-coil (Reese et al. 2003). A high-resolution ( $1 \text{ mm}^3$ ) 3D magnetization-prepared rapid acquisition with gradient echo scan was acquired on these participants.

Automated cortical parcellation was performed in each participant's T1 scan, using the Destrieux atlas (Destrieux et al. 2010) from Freesurfer 5.1 (Fischl et al. 2002, 2004) to define 148 cortical regions. Automated parcellation results were reviewed for quality control and were then registered to each individual's diffusion images using Freesurfer's *bregister* function, which uses surface-based algorithms to register images, and we initialized the registration with FSL's FLIRT. We used the DWI-registered parcels as seed and target regions for fiber tracking. The resulting cortical targets were then checked and corrected for automatic parcellation or segmentation errors if necessary. The principal diffusion directions were calculated per voxel, and probabilistic diffusion tractography was carried out using FSL-FDT (Behrens et al. 2007) with 5000 streamline samples in each seed voxel to create a connectivity distribution to each of the target regions, while avoiding a mask consisting of the ventricles. Each of the 148 regions was used as a seed region and tractography was carried out to all 147 remaining regions, or targets. Thus, every voxel within each parcel is described by a vector of connection probabilities to each other brain region.

### fMRI Acquisition Parameters and Analysis

Stimuli for the fMRI consisted of 3-s movie clips of faces, bodies, scenes, objects, and scrambled objects. Movies of faces and bodies were filmed against a black background and framed to reveal

just the faces or bodies of 7 individuals, shown one at a time. Scenes consisted primarily of pastoral scenes filmed through a car window while driving slowly through the countryside or suburb. Objects were selected specifically to minimize any suggestion of animacy of the object itself or of an invisible actor pushing the object. Scrambled object clips were constructed by dividing each object movie clip into a  $15 \times 15$  box grid and spatially rearranging the location of each of the resulting boxes. Pilot testing indicated that a contrast of the response for moving faces versus moving objects identified the same fusiform face area (FFA) as that identified in a standard static localizer. Further studies show that the FFA responds similarly to movies of faces as to static snapshots of faces (Pitcher et al. 2011).

Functional data were acquired over 4 block-design functional runs (gradient echo sequence 2000 ms TR, 30 ms TE,  $90^\circ$  flip, 234 volumes,  $3 \times 3 \times 3$  mm voxel size). Each functional run contained three 18-s fixation blocks at the beginning, middle, and end of the run. During these blocks, a series of 6 uniform color fields were presented for 3 s each. Each run also contained 2 sets of 5 consecutive stimulus blocks (faces, bodies, scenes, objects, or scrambled objects) sandwiched between these rest blocks, resulting in 2 blocks per stimulus category per run. Each block lasted 18 s and contained 6 3-s movie clips from each of the 5 stimulus categories. The order of stimulus category blocks in each run was palindromic, and specific movie clips were chosen randomly to be presented during the block. Participants were asked to passively view the stimuli.

Functional data were analyzed with FSL software (<http://www.fmrib.ox.ac.uk/fsl/>). Images were motion corrected, smoothed (5-mm Gaussian kernel, full-width at half-maximum) and detrended, and were fit using a standard gamma function ( $d = 2.25$  and  $t = 1.25$ ). Data were not spatially normalized. Statistical modeling was then performed using a general linear model on the preprocessed functional images. Next, t-maps corresponding to each contrast of interest were overlaid on each participant's high-resolution anatomical image. The contrasts were as follows: Faces > Objects, Bodies > Objects, Scenes > Objects, Objects > Scrambled objects.

Each participant's functional image for each contrast was registered to his or her DWI using Freesurfer's `bbregister` and initialized using FSL's `FLIRT`. Because we were interested in predicting relative activation values that were independent of task-specific parameters such as the degrees of freedom, we standardized the t-statistic values across all gray-matter parcels per participant. For each anatomical parcel, the mean functional value across the brain was subtracted from each voxel and divided by the standard deviation. The standardized value per voxel was then used for the subsequent regression models, which were built per region. Thus, every voxel is now also described by a vector of t-statistics for each functional contrast.

## Modeling Approach

Subjects were divided into 2 groups (group 1 for leave-one-out cross-validation and group 2 for replication); this procedure ensures that any relationship learned from one set of data is separate from the data that is used to assess the accuracy of that learnt relationship (Hastie et al. 2009).

### Group 1

To predict function from connectivity, we used a leave-one-subject-out cross-validation (LOOCV) routine, in which we excluded a single subject whose data we wish to predict, trained a model with all of the remaining subjects, and then applied the model to the left-out subject. This routine was repeated for all subjects,

generating independent predictions for all subjects. Each seed parcel is modeled as follows (Fig. 1): every voxel of the modeled region (i.e., seed parcel) has a neural response to a given functional contrast. Every voxel also has a 148-dimensional vector of connection probabilities to each other brain parcel (targets). We then concatenate all of the native-space voxels from each subject's seed parcel (excluding all voxels of the left-out subject), to produce 1) a vector of all seed voxels' neural responses (length  $N$  voxels) and 2) a matrix of connectivity vectors for each of these voxels ( $N \times 148$ , where rows are voxels and columns are connection probabilities to each target parcel). We used a linear regression to model the relationship between the fMRI contrast response of each voxel, and the 148-dimensional vector of connectivity for each voxel. Because all analyses were performed on subject-specific anatomy, the number of voxels in a given parcel varied among individuals. However, because each voxel was an independent observation in the regression, the model could learn the relationship between the fMRI response and the 148-dimensional vector of connectivity of each voxel (Fig. 1b). It is also important to note that there was no identifying or matching of spatial location of voxels across participants. Further, the model was blind to the participant each voxel belonged to. This modeling step resulted in a 148-dimensional vector of predictive coefficients ( $f(x)$ ; Figure 1e; note that the coefficient for the modeled parcel's connectivity with itself is undefined because within-parcel connectivity was not included). These coefficients are weights that reflect the relevance of each target parcel's connectivity in predicting neural responses in the seed. The left-out participant also has a connectivity matrix of  $N_i$  voxels  $\times$  148 parcels (i.e., connectivity from every voxel of the left-out participant's seed parcel to each target parcel). We predicted the neural responses for this left-out subject by applying the coefficients  $f(x)$  to each voxel's 148-dimensional connectivity vector, resulting in a predicted fMRI value for every voxel of the seed parcel.

In order to generate predictions for the entire brain, this procedure, from tractography to prediction, was repeated for every parcel, and concatenated. This was then compared with the participants' own observed fMRI images for that contrast, and absolute errors (AEs) were calculated (absolute value of actual - predicted per voxel).

### Group 2

Cross-validation routines ensure independent data modeling for each fold (i.e., the left-out subject is completely excluded from the modeling procedure based on the remaining subjects). However, because the  $n - 1$  data are used to model all other folds, cross-validation procedures have a potential for over-fitting, and may be more optimistic than fully independent test groups. Therefore, we built an independent test group of participants. For each anatomical parcel, we generated a final linear regression model from all of the group 1 subjects' connectivity and fMRI data. We applied this final model of the relationship between connectivity and function, to each group 2 subjects' connectivity data, to produce predicted fMRI maps per subject. Prediction accuracies were calculated by comparing these predictions with each participant's actual fMRI values (errors were calculated in the same way as for group 1). The accuracies were tested against random permutations and other benchmarks (below). We also performed a one-way ANOVA on the mean AE across all gray-matter voxels per subject for all of the functional contrasts to discover whether any contrasts were better predicted by connectivity than the others; post hoc t-tests were used to identify the contrasts that were significantly better predicted than others (at  $P < 0.05$  Bonferroni corrected for 6 pair-wise comparisons).

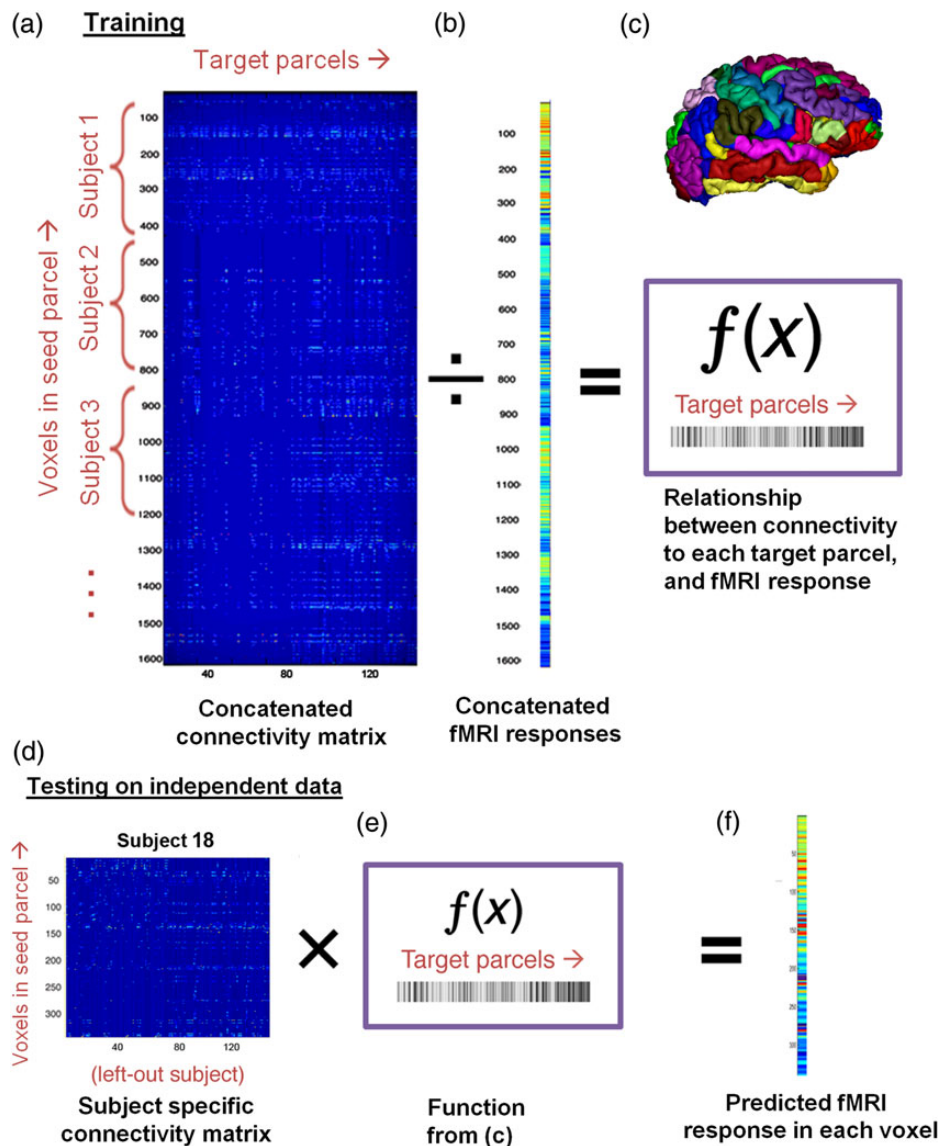


**Figure 1.** Schematic of processing pipeline. Each individual's anatomical image is first divided into 148 parcels, shown on the colored brain. For each parcel, the following procedure is carried out (i.e., each parcel is modeled separately). (a) Connectivity from each seed voxel to every other parcel is calculated for each individual, and the connectivity matrices from all individuals except for one (the left-out subject) are concatenated. Voxels are shown in rows (this number will vary for each individual) and the 148 target parcels are in columns; connection probability is depicted in color. (b) Concatenate the fMRI response (depicted as a colored vector) to the contrast of interest (e.g., Faces > Objects) such that every voxel is matched with its vector of connectivity in (a). (c) A linear regression (represented as  $\pm$ ) models the relationship between (a) and (b). This relationship ( $f(x)$ ) is a vector of coefficients the same length as the number of columns in (a). It reflects the contribution of each target parcel to predicting fMRI responses, and is depicted as the grayscale vector. (d) The left-out participant also has a connectivity matrix of  $n$  voxels  $\times$  148 parcels. (e)  $f(x)$  is applied to each voxel in the left-out participant's connectivity matrix, which yields (f) a predicted fMRI response for every voxel. Thus, the left-out participant now has an fMRI response that is predicted from his/her own DWI connectivity alone. The predicted responses are then compared with that participant's actual fMRI responses per voxel. Every participant is left-out iteratively such that independent predictions are generated for each participant, in their own native space. This procedure is repeated for each parcel, and for each contrast. After all of group 1 participants have been predicted, a final  $f(x)$  is learned from all the participants (i.e., no one is left-out). This final  $f(x)$  is then applied to new participants from an independent group (group 2). Steps (d-f) are thus repeated for each group 2 participant to generate predicted fMRI responses for every voxel, for every parcel, and for every contrast.

### Connectivity-Based Predictions of Neural Responses across All Gray-Matter Voxels

As a measure of performance accuracy, we measured the AE per voxel (reported in standardized units) per participant, by calculating the absolute difference between the predicted and actual values (AE, also see above). We compared the prediction accuracies with a benchmark model to further test whether connectivity can predict function beyond what can be predicted from a group analysis (see Saygin et al. (2012) for details).

The group models were also made through LOOCV. Each participant's functional data were spatially normalized into Montreal Neurological Institute space with FreeSurfer's surface-based `bbregister` and FSL's `FNIRT`, checked, and corrected for registration errors, and superimposed to create composite maps. We performed a random-effects test on whole-brain fMRI data with SPM8 on each contrast image from all but one participant. The resulting t-statistic image, which was based on all the other participants in normalized space, was applied to the participant left out of the group analysis

and was registered back into his or her native space. This resulted in a predicted value for each voxel. A final group-average t-statistic was also generated from all of the group 1 participants, and this group-average map was applied to each of the group 2 subjects to evaluate group-based prediction accuracies of function. We performed a pair-wise t-test of mean absolute and squared prediction errors of all gray-matter voxels across the participants in groups 1 and 2 separately.

### Connectivity-Based Predictions of Neural Responses Within Regions of Interest

For each contrast, we then registered each subject's actual and predicted fMRI maps (based on the group-average and connectivity analyses separately) to a common Freesurfer CVS atlas (Postelnicu et al. 2009; Zöllei et al. 2010). The probabilistic parcels of ROIs (based on a large independent sample of adults, Julian et al. 2012) were created in this CVS space, and we calculated prediction accuracies for connectivity versus group average within each of these ROIs. In this way, each of the ROIs was comparable in size across participants. We performed a pair-wise t-test per participant across all gray-matter voxels within each of the ROI parcels. A Bonferroni-corrected criterion threshold of  $P < 0.05/(26 \times 19)$  (total number of subjects in both groups times number of ROIs) was used to report the number of participants whose activation pattern was better predicted by one model versus another.

### Parcels with the Strongest Relationship Between Connectivity and Function

We next examined the model coefficients in order to determine which parcels have the strongest relationship between their pattern of connectivity and neural selectivity. For each functional contrast, we produced a final connectivity model from all the subjects in group 1 and evaluated each anatomical parcel's model  $R^2$ . The  $R^2$  is a standard metric of goodness of fit, and for these data, it reflects the proportion of the variance in fMRI activity that was accounted for by connectivity, across all of the voxels in the region and across all subjects (the model is agnostic to which voxels belong to which subject).  $R^2$  is especially useful for comparisons across parcels, as it is standardized and bound between 0 and 1; by comparison, mean absolute error (MAE) is not standardized and unbounded, and reflects prediction performance rather than the multivariate relationship between connectivity and function. We separately correlated each parcel's  $R^2$  with 2 metrics: 1) functional selectivity and 2) accuracy of multi-voxel pattern analysis (MVPA; see Haxby et al. 2001), which reflect how well the response patterns across voxels within a parcel are able to differentiate between each functional condition. We calculated functional selectivity by identifying the 5th percentile voxels (based on t-statistic responses to each functional contrast) from 3 of 4 functional runs, and averaging the responses of these voxels from the remaining functional run. We repeated this procedure 4 times, iterating which run was left out, and averaged the 5th percentile functional contrast responses across all of these iterations. Thus, the measure of functional selectivity was generated independently from the data that was used to identify the top responding voxels, and was also less susceptible to noisy spikes in fMRI data. In this way, we identified the functional selectivity of each anatomical parcel to each functional contrast and could assess the extent to which the functional selectivity of a parcel was related to how well connectivity could predict function.

### Functionally Relevant Networks for Predicting Neural Responses

For each parcel and for each contrast, we generated a final model using all of the subjects from group 1 (see above). This model yielded a set of predictive coefficients ( $f(x)$ ), which was a 148-dimensional vector. This vector reflected the weight or contribution of each target's connectivity in predicting responses in the seed parcel. Some of these connections were significant predictors, and others were not. We binarized the predictive coefficients based on Bonferroni-corrected significance, and concatenated these vectors across all parcels. This resulted in a  $148 \times 148$ -dimensional affinity matrix for each functional contrast, or the functionally relevant network (FRN) for that contrast. There were a total of 4 affinity matrices (one per contrast). A row of this matrix represents a single parcel, and its columns reflect whether each other region significantly predicts this parcel's neural activity: significant predictors are represented by ones and nonsignificant predictors are represented by zeroes. We can depict this matrix as a network, with predictors as sources and the regions that they predict as sinks (i.e., arrows originate from predictors and point toward the regions that they predict). This complex network offers valuable information about the influence of each parcel on predicting responses across the brain. We used various graph theoretical measures to quantify the contribution of each parcel in predicting connectivity, and we related these measures to the functional selectivity of the parcels.

The regression models know nothing about the function of each of these predictive parcels; the model is built only on the fMRI response of each voxel within the seed parcel, and each seed voxel's connectivity with the target parcels (not the fMRI response of these target parcels). But we were interested in exploring 1) whether the most common predictive parcels are the most functionally selective for a given contrast, 2) whether the predictors are predictive of each other and form cliques of functionally selective parcels that are predictive of one another, and 3) whether the most embedded predictors (i.e., the foundations or cores of the FRN) are the most selective. For each contrast, we calculated each parcel's degree, clustering coefficient, and core number, and correlated these measures with the functional selectivity of the parcels. This functional selectivity measure was identical to what was used in the previous section (see Parcels with the Strongest Relationship Between Connectivity and Function); briefly, we identified the top 5% voxels based on 3/4 runs, averaged the functional responses of those voxels in the left-out run, iterated which run was left out, and averaged the 5th percentile functional contrast responses across all of these iterations, and then across all subjects.

A parcel's degree is the number of other parcels that are predicted by connectivity to that given parcel. In other words, it measures how often a parcel's connectivity predicts function elsewhere. To calculate each parcel's degree for each contrast, we summed each column of the affinity matrix for each contrast, which again is binary and defines what parcels are predictive of each other parcel. We also calculated the clustering coefficient for each parcel (see Watts and Strogatz 1998). The clustering coefficient for a given parcel is based on its neighbors (i.e., the other parcels it predicts and the parcels that are predicted by it). The clustering coefficient for each parcel is the proportion of that parcel's neighbors that are themselves neighbors. It is equal to the number of edges between a parcel's neighbors divided by all possible edges among those neighbors. The clustering coefficient ranges from 0 to 1, where 0 indicates that none of a parcel's

neighbors predict one another, and 1 indicates that all of a parcel's neighbors are predictive of each other. Finally, we implemented k-core decomposition (Lick and White 1970; Seidman 1983), in which, for increasing integers in  $k$ , parcels are removed recursively until all parcels in the remaining subnetwork have a degree of at least  $k$ . Each parcel is then assigned a core number, which is the largest  $k$ -core that a parcel belongs to. More detailed information about this procedure can be found in Hagmann et al. (2008) and Alvarez-Hamelin et al. (2005).

## Results

We divided each individual's native anatomical brain image into a common set of 148 cortical parcels using the Destrieux atlas (Destrieux et al. 2010) from Freesurfer 5.1 (Fischl et al. 2002, 2004). These parcels are defined separately for each individual, and retain individual anatomical variations. By establishing the correspondence of each anatomical parcel across subjects, this method enables us to define the connectivity of each voxel in a common currency across subjects: the strength of the connection of that voxel to each of the 147 other parcels. We can thus derive from one set of subjects the voxel-wise relationship between function and connectivity (to all 147 other parcels), and then apply this relationship to new individuals, predicting the functional responses of each voxel in each new subject from the diffusion-based connectivity of that voxel to the 147 other parcels. We compared the resulting DWI connectivity-based predictions of fMRI responses (i.e.,  $t$ -statistic contrast values) to each participant's actual fMRI values for that contrast, and evaluated the accuracy of the predictions with respect to a group-average benchmark. We first assessed how well connectivity predicts function across all gray-matter voxels (see Connectivity-Based Predictions of Neural Responses across All Gray-Matter Voxels). We next compared connectivity-based versus group-average voxel-wise prediction accuracies within selective regions of interest (ROIs) that were defined based on an independent dataset (see Connectivity-Based Predictions of Neural Responses Within Regions of Interest). We then asked whether connectivity is especially predictive of function in parcels with the most reliable fMRI responses (see Parcels with the Strongest Relationship Between Connectivity and Function). Finally, we analyzed the subset of connections that best predicted voxel-wise functional activation, or the FRN for each visual domain across cortex [see Functionally Relevant Networks for Predicting Neural Responses].

### Connectivity-Based Predictions of Neural Responses across All Gray-Matter Voxels

We concatenated the voxel-wise predictions of fMRI contrast responses across all parcels, and calculated prediction accuracy for all cortical gray-matter voxels. The contrast for "Faces" (Faces > Objects) typically elicits activation in the posterior superior temporal sulcus, and in ventral temporal and occipital regions known as the FFA and occipital face area (Table 1). Figure 2a illustrates the results for a representative subject. The predicted response (Fig. 2a), built solely from the same subject's connectivity data, is strikingly similar to the actual response. This result demonstrates that an individual's response pattern to Faces can be well predicted by that individual's connectivity pattern.

To quantify prediction accuracy, we measured prediction errors in each individual's native anatomy (in diffusion space). We calculated the AE per voxel as the difference between the predicted contrast  $t$ -statistic and actual fMRI images, and MAE as a

**Table 1** Functional domains with corresponding specialized brain regions (fROIs)

Function	fROIs
Face perception	Fusiform face area, FFA Occipital face area, OFA Superior temporal sulcus, STS
Body perception	Extrastriate body area, EBA Fusiform body area, FBA
Scene perception	Parahippocampal place area, PPA Transverse occipital sulcus, TOS Retrosplenial cortex, RSC
Object perception	Lateral occipital, LOC Posterior fusiform sulcus, PFS

measure of accuracy for each contrast averaged over all gray-matter voxels (Fig. 3a). Because group analyses are currently the only alternative means of predicting voxel-wise neural responses in a new participant, they were chosen as benchmark models that connectivity-based predictions should meet or exceed in order to be considered useful. These group-average models also yielded voxel-wise predictions of fMRI activation, and were compared with the voxel-wise predictions from connectivity. Across all gray-matter voxels, connectivity significantly outperformed the group-average predictions for the first group of participants (i.e., cross-validation group) in predicting responses to faces ( $T_{17} = -45.13$ ,  $P = 3.84 \times 10^{-19}$ ). Further, the connectivity-based predictions were comparable with the fMRI scan-rescan reliability in 5 participants who were functionally scanned on 2 separate occasions (Supplementary Fig. 1).

Next, we evaluated the connectivity-based predictions in an independent test group of participants (group 2; Fig. 3b) because we wanted to ensure replicability and prevent model overfitting (see Materials and Methods). We again found that connectivity outperformed benchmark models across all gray-matter voxels, for Faces ( $T_7 = -21.24$ ,  $P = 1.29 \times 10^{-7}$ ). These results replicate the previous findings from Saygin et al. (2012), where connectivity predictions outperformed the group-average benchmark predictions in the fusiform for Faces > Scenes, and extend the findings for the whole cortex and for the contrast of Faces > Objects.

The contrast for "Bodies" (Bodies > Objects) localizes the functionally defined regions known as the extrastriate body area and the fusiform body area (FBA). Again, a subject's own connectivity patterns are capable of predicting the landscape of body selectivity in and around these regions (Fig. 2b). Across all gray-matter voxels, we found that connectivity-based predictions were more accurate than group-based predictions for group 1 ( $T_{17} = -31.50$ ;  $P = 1.62 \times 10^{-16}$ ) as well as for another group of participants (group 2:  $T_7 = -20.56$ ;  $P = 1.62 \times 10^{-7}$ ).

"Scenes" (Scenes > Objects) typically evoke activity along the ventral medial surface (e.g., Swards 2011). Some of the functional regions often associated with scene selectivity are the parahippocampal place area and retrosplenial cortex, and again we see that a subject's connectivity pattern alone is highly predictive of their pattern of functional response (Fig. 2c). We found that connectivity was a better predictor than group activations of functional responses voxelwise across the whole brain in group 1 ( $T_{17} = -27.12$ ;  $P = 1.97 \times 10^{-15}$ ) as well as in group 2 ( $T_7 = -20.31$ ;  $P = 1.76 \times 10^{-7}$ ).

"Objects" (Objects > Scrambled Objects) result in a distributed set of functional regions collectively known as the lateral

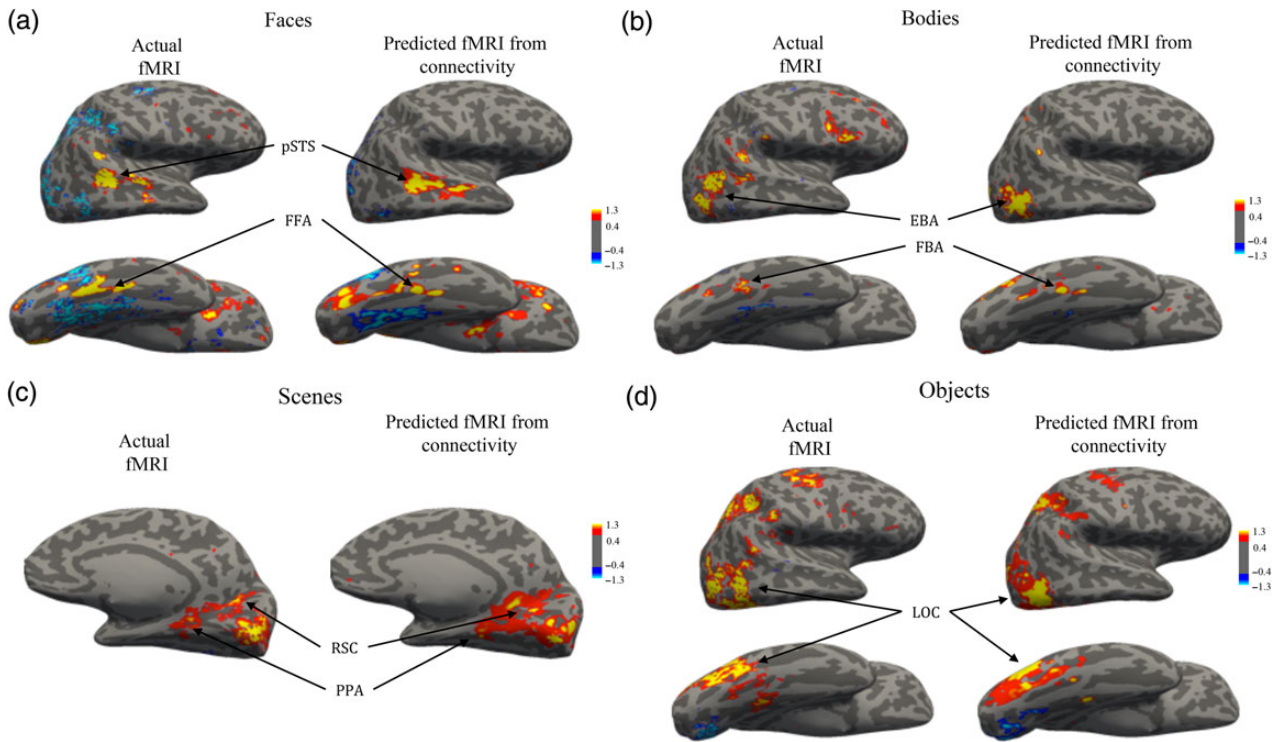


**Figure 2.** Visualization of prediction results on an example subject. Representative subject's actual and predicted activation images are up-sampled from the DWI structural image to the same participant's structural scan, and projected onto the participant's inflated brain surface. Predicted fMRI activation values (right column of each panel) for each visual category contrast closely match the actual fMRI values (left columns) for that contrast, especially in regions commonly identified as being functionally selective for that particular visual category (i.e., ROIs; see Table 1). (a) Faces (b) Bodies (c) Scenes (d) Objects.

occipital complex. Not only can connectivity capture this robust neural response (Fig. 2d), but it also accounts for the somewhat less characterized dorsal activity patterns, for example in the intraparietal sulcus. Connectivity versus group-average comparisons again indicated that connectivity predictions were more accurate across all gray-matter voxels of the brain, in both group 1 (Fig. 3a;  $T_{17} = -18.81$ ;  $P = 8.16 \times 10^{-13}$ ) and group 2 (Fig. 3b;  $T_7 = -17.79$ ;  $P = 4.37 \times 10^{-7}$ ).

A one-way ANOVA found significant differences in prediction errors between the 4 contrasts ( $F_3 = 14.71$ ,  $P = 1.75 \times 10^{-7}$ ). Post hoc t-tests revealed that the connectivity-based predictions for Bodies had significantly higher errors than each of the other contrasts (Bodies vs. each of: Faces  $t = 9.08$ ,  $P = 6.24 \times 10^{-8}$ ; Scenes  $t = 5.73$ ,  $P = 2.43 \times 10^{-5}$ ; Objects  $t = 5.38$ ,  $P = 4.94 \times 10^{-5}$ ). Additionally, Faces and Scenes were significantly more accurate than Objects ( $t = 2.87$ ,  $P = 1.07 \times 10^{-2}$ ;  $t = 3.50$ ,  $P = 2.72 \times 10^{-3}$ , respectively). Faces and Scenes prediction errors were not significantly different from one another. Furthermore, these results were replicated in group 2 ( $F_3 = 5.15$ ;  $P = 5.83 \times 10^{-3}$ ; Supplementary Table 1 for pair-wise post hoc tests).

### Connectivity-Based Predictions of Neural Responses Within Regions of Interest

We tested whether connectivity was able to capture voxel-wise contrast responses not only across the brain, but also in the most functionally specific regions (i.e., ROIs; Table 1). We defined ROIs for each subject using parcels from Julian et al. (2012), and evaluated the voxel-wise prediction accuracies of the connectivity and the group-average (benchmark) models in each ROI. We also compared prediction errors for each voxel

within the ROIs of each participant (i.e., within-subject paired t-test on voxel-wise errors for connectivity vs. group predictions). We calculated the percentage of subjects whose connectivity patterns better predicted fMRI activation than the group average ( $P < 0.05$  Bonferroni corrected for total number of ROIs by total subjects in both groups, i.e., 19 ROIs  $\times$  26 subjects). With the exception of right fusiform body area, the voxel-wise responses within each ROI were significantly better predicted by connectivity patterns than a group average in over 90% of subjects (Fig. 4a). The results were replicated in group 2, with over 90% of the subjects' fMRI activation significantly better predicted by connectivity than by group in each ROI (Fig. 4b). Thus, even within the immediate vicinity of each ROI, connectivity-based predictions of function were a better proxy for an individual's fMRI responses than current alternatives for estimating function (i.e., group average).

### Parcels with the Strongest Relationship Between Connectivity and Function

Next, we examined the relationship between connectivity and function (i.e., goodness of fit) for each anatomical parcel, and whether the strength of this connectivity-function relationship could be explained by the functional characteristics of the anatomical parcels. We used 2 metrics to describe each parcel's functional characteristics: 1) the functional selectivity of the parcel, calculated from the top 5th percentile voxels for each functional contrast; and 2) the functional information that is present in each parcel (i.e., MVPA decoding accuracy). We wanted to know if there was any systematic relationship between goodness of fit (between functional responses and connectivity) and the

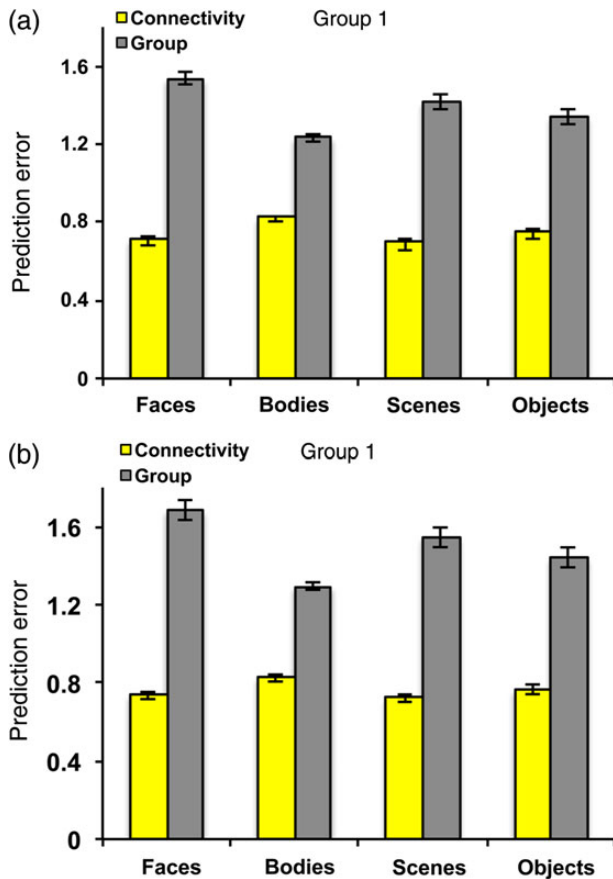


**Figure 3.** Mean prediction errors and comparison to benchmark. Prediction errors (i.e., mean absolute errors) across all voxels for the predicted fMRI activation by connectivity and the group-average benchmark are plotted for each functional contrast for participants in (a) group 1 and (b) group 2. For both groups 1 and 2, predictions from the connectivity models were significantly more accurate (lower error) than predictions from the group-analysis benchmark.

functional characteristics of parcels. For example, do the most selective parcels have the strongest relationship between connectivity and function, or are some parcels especially “wired” for function, regardless of selectivity?

We calculated each parcel’s goodness of fit ( $R^2$ ), which captures the degree to which connectivity can explain a parcel’s functional variance across voxels and subjects. We first correlated these  $R^2$  values with the functional selectivity of each parcel. For each contrast and for each parcel, we identified the most selective voxels (i.e., voxels with 5th percentile responses based on the contrast  $t$ -statistic) from 3 of 4 functional runs, and recorded the contrast responses of these voxels from the remaining functional run. We repeated this procedure 4 times (iterating which run was left out), and averaged across these iterations. Thus, our measure of functional selectivity was generated independently from the data that was used to identify the top responding voxels. We found that the  $R^2$  values were positively and significantly correlated with functional selectivity for all 4 of the functional contrasts (Fig. 5): Faces:  $r = 0.46$ ,  $P = 3.34 \times 10^{-9}$ ; Bodies:  $r = 0.40$ ,  $P = 3.48 \times 10^{-7}$ ; Scenes:  $r = 0.66$ ,  $P = 8.94 \times 10^{-20}$ ; and Objects:  $r = 0.63$ ,  $P = 6.35 \times 10^{-18}$ .

We next investigated whether the fit of connectivity to function could also be explained by the amount of contrast-specific information present in the pattern of functional responses across the voxels of each parcel. For each parcel, we asked how well the voxel-wise pattern of responses was able to distinguish one

functional contrast from the others (i.e., decoding accuracy through MVPA, e.g., Haxby et al. 2001). These MVPA accuracies reflect the pattern (and cross-run reliability) of responses for all voxels in a parcel, and how unique that pattern is for that contrast (i.e., how well can the pattern decode the contrast of interest versus the rest). We found that MVPA decoding accuracies for each functional contrast were also positively and significantly correlated with the  $R^2$  values of the parcels (Fig. 6): Faces:  $r = 0.38$ ,  $P = 2.26 \times 10^{-6}$ ; Bodies:  $r = 0.38$ ,  $P = 2.24 \times 10^{-6}$ ; Objects:  $r = 0.57$ ,  $P = 4.91 \times 10^{-14}$ ; Scenes:  $r = 0.56$ ,  $P = 1.63 \times 10^{-13}$ .

We also compared  $R^2$  values for sulcal versus gyral parcels to check whether DWI connectivity performed better in certain parcels simply because of gyral bias. We found that there were no differences for any contrast (Faces:  $P = 0.20$ ; Bodies:  $P = 0.27$ ; Objects:  $P = 0.66$ ; Scenes:  $P = 0.15$ ).

### Functionally Relevant Networks for Predicting Neural Responses

We identified the connections that were significant predictors of function for each anatomical parcel, and for each functional contrast. When pooled across all anatomical parcels, these significant predictors comprise a complex network that has been distilled to only those connections that are predictive of each function; we define these networks as the FRNs. There were 4 networks (one per contrast). The complete FRNs for each contrast are shown in Figure 7 (see also Supplementary Fig. 2). We analyzed the FRNs using graph theoretical approaches, which provide a powerful way to quantify complex networks (see Fig. 8, also Bullmore and Sporns 2009). We calculated each predictor’s parcel’s degree, clustering coefficient, and core number, and correlated these measures with the functional selectivity of the parcels (same selectivity measure that was used in see Parcels with the Strongest Relationship Between Connectivity and Function).

Are the most common predictors also the most functionally selective? We calculated the number of times each parcel was predictive of functional responses in every other parcel (in graph theoretical vocabulary, the parcel’s degree), and correlated these results with the functional selectivity of the parcels. For all contrasts except Bodies, we found that the more selective a parcel is for a given category, the more often connectivity to that parcel is predictive of selectivity for that category (Faces:  $r = 0.29$ ,  $P = 3.98 \times 10^{-4}$ ; Bodies:  $r = 0.14$ ,  $P = 0.0952$ ; Scenes:  $r = 0.28$ ,  $P = 4.47 \times 10^{-4}$ ; Objects:  $r = 0.36$ ,  $P = 6.07 \times 10^{-6}$ ).

To further analyze the FRNs, we calculated another metric commonly used in graph theory: the clustering coefficient of each parcel. The clustering coefficient measures how interconnected the secondary network of a node is. For example, a node with a high clustering coefficient would be part of a clique, such that the nodes that connect to it are also connected to one another. To illustrate this metric for FRNs, a parcel with a high clustering coefficient may predict function in a set of other parcels, and these parcels would also predict function in one another. We correlated each parcel’s clustering coefficient with its degree of selectivity. For all 4 contrasts, we observed a significant positive correlation between clustering and selectivity (Faces:  $r = 0.26$ ,  $P = 1.15 \times 10^{-3}$ ; Bodies:  $r = 0.26$ ,  $P = 1.55 \times 10^{-3}$ ; Scenes:  $r = 0.34$ ,  $P = 2.24 \times 10^{-5}$ ; Objects:  $r = 0.30$ ,  $P = 2.09 \times 10^{-4}$ ). Thus, the most selective parcels form local cliques such that their connectivity to one another is especially predictive; conversely, nonselective parcels are more diffuse and do not form predictive communities.

We next performed  $k$ -core decomposition (Lick and White 1970; Seidman 1983), which identifies the underlying backbone of a network through iterative pruning (i.e., removing nodes

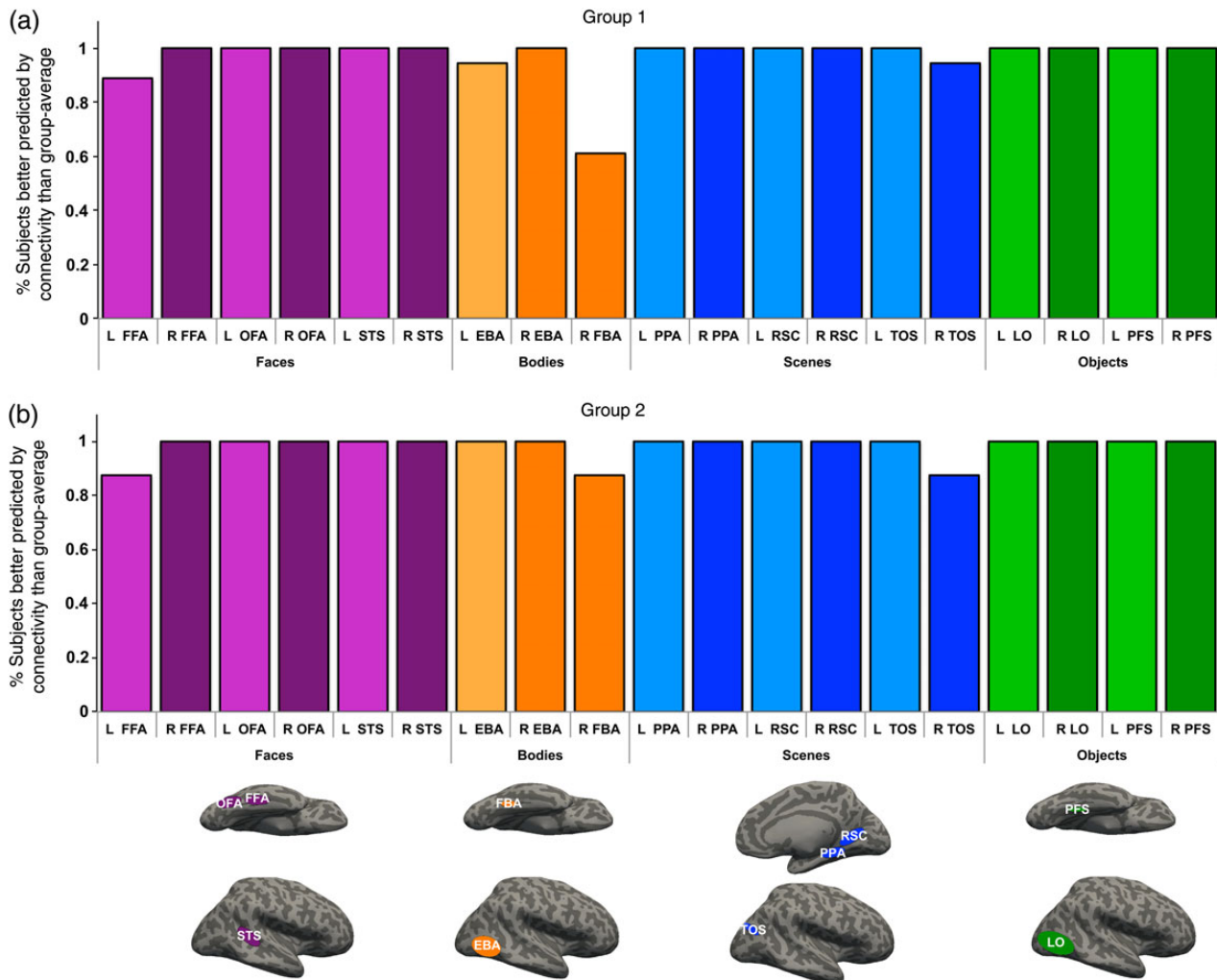


**Figure 4.** Predictive accuracy across subjects for connectivity versus group-analysis benchmark. For each of the fROIs (depicted on the inflated brains, see Julian et al. (2012) for ROI nomenclature), we calculated the percentage of subjects whose connectivity patterns better predicted their activation patterns than a group-based prediction (paired *t*-test of voxel-wise prediction errors for connectivity vs. group average per subject,  $P < 0.05$  Bonferroni corrected for total number of fROIs times the total number of subjects across both groups, i.e.,  $26 \times 19$ ) in (a) the cross-validation group (group 1) and (b) replication test group (group 2). Lighter colors indicate left-hemisphere fROIs (some fROIs did not have a left-hemisphere counterpart).

from the network). In *k*-core decomposition, several subnetworks (called *k*-cores) are identified by successively removing all nodes of a network with degree smaller than *k* until all remaining nodes have a degree equal to or larger than *k* (e.g., remove a parcel with the lowest degree, see if its neighbors are connected with any other parcel, remove the neighbors too if they now have a low degree, etc.). Each successive *k*-core contains increasingly robust nodes and the largest *k*-cores constitute the structural backbone of a network (e.g., Hagmann et al. 2008). Using this approach, we computed the core number for each parcel; parcels with larger *k*-cores would thus constitute the deepest foundations of the FRNs. We wanted to know whether the foundations of the FRNs were also the most selective for each contrast, so we correlated each parcel's core number with its selectivity. For all 4 contrasts, we observed a significant positive correlation between core number and selectivity (Faces:  $r = 0.36$ ,  $P = 8.18 \times 10^{-6}$ ; Bodies:  $r = 0.23$ ,  $P = 4.79 \times 10^{-3}$ ; Scenes:  $r = 0.30$ ,  $P = 2.22 \times 10^{-4}$ ; Objects:  $r = 0.47$ ,  $P = 1.55 \times 10^{-9}$ ). Thus, the central core of the FRNs is composed of the most selective parcels; conversely, nonselective parcels make up the more peripheral components of the FRNs.

## Discussion

We hypothesized that extrinsic anatomical connectivity mirrors functional selectivity at a fine spatial grain (voxelwise) across the human cortex, such that the unique connectivity fingerprint of voxels may be used to predict neural responses throughout the brain, and across many functions. We tested this hypothesis for high-level visual functions using a novel method of directly linking DWI and fMRI in the same individuals (Saygin et al. 2012).

### Connectivity Can Predict Neural Selectivity at a Voxel-Wise Scale

For each functional contrast, we found that voxel-wise fMRI activity of an individual can be predicted using only their DWI connectivity patterns. There is great functional diversity within cortical regions and our results demonstrate that specific connectivity patterns may be important for this functional diversity at a fine spatial grain. Future studies may use the present approach to gain a more detailed understanding of the

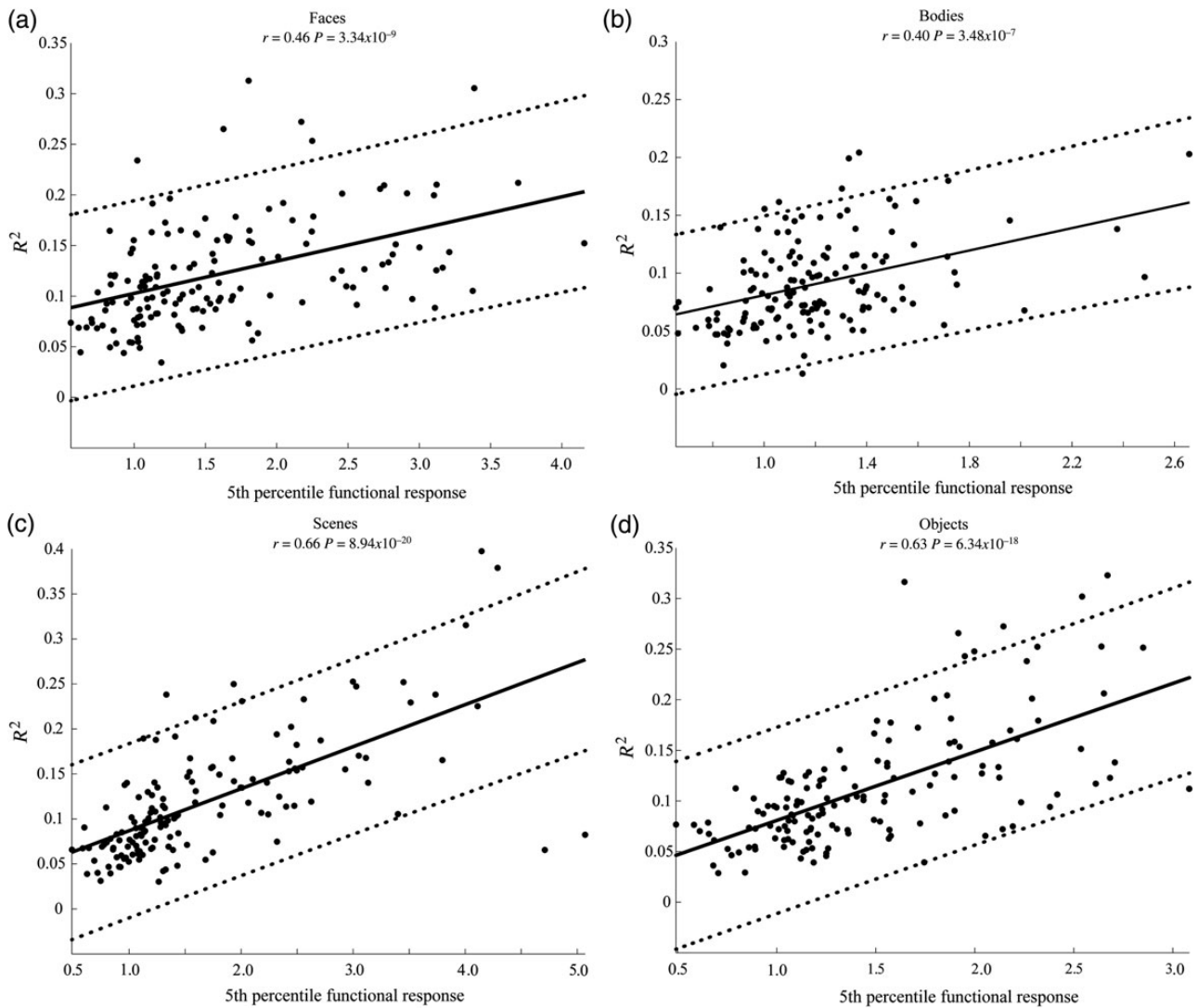


**Figure 5.** Model fits positively correlate with functional selectivity per anatomical parcel. The fits or  $R^2$  values for the final models of connectivity and function per anatomical region were significantly and positively correlated with the mean absolute contrast responses for voxels in the 5th percentile for each parcel. These values reflect the response selectivity of each parcel to the functional contrast, (a) Faces, (b) Bodies, (c) Scenes, and (d) Objects. Parcels with better model fits had greater functional selectivity for that functional contrast.

structure-function relationship of voxel-wise preferences for specific stimuli or selectivity for subordinate categories (e.g., individual faces or specific body parts).

Further, by treating each voxel as a unique entity in both connectivity and function, this approach can be used to explore the gradient of functional responses across the cortex while remaining agnostic about whether discrete brain modules exist. Future studies can explore the topology of connectivity profiles in greater detail and discover whether connectivity fingerprints exhibit sharp spatial boundaries that may correspond with the boundaries of putative functional modules.

### Connectivity Can Predict Neural Selectivity Throughout Human Cortex

These results replicate prior work showing that the fusiform gyrus has specialized connectivity patterns that underlie face perception (Saygin et al. 2012). But importantly, these findings demonstrate that the tight relationship between connectivity

and function also exists across other components of the face processing network. Further, by modeling selectivity as a function of connectivity across the brain, we were able to compare the relationship between neural selectivity and model fit across anatomical parcels. This allows us to address whether this relationship 1) holds equally across cortical regions, 2) is specific to certain parcels, or 3) is strongest in the most selective parcels. Our data show a tight relationship between connectivity and function across the cortex, but a stronger relationship for each contrast in parcels that contain the greatest selectivity for that contrast. Thus, some of the strongest predictions were found for face selectivity around the fusiform gyrus where connectivity accounted for 30% of the functional variance across voxels and across participants, and for object selectivity in lateral occipital cortex, where connectivity accounted for 32% of the functional selectivity across voxels. These results indicate that extrinsic connectivity bears a close relationship to functional selectivity across the cortex.

Although the model fits increased with the selectivity of the parcel for the contrast in question, it is difficult to disentangle

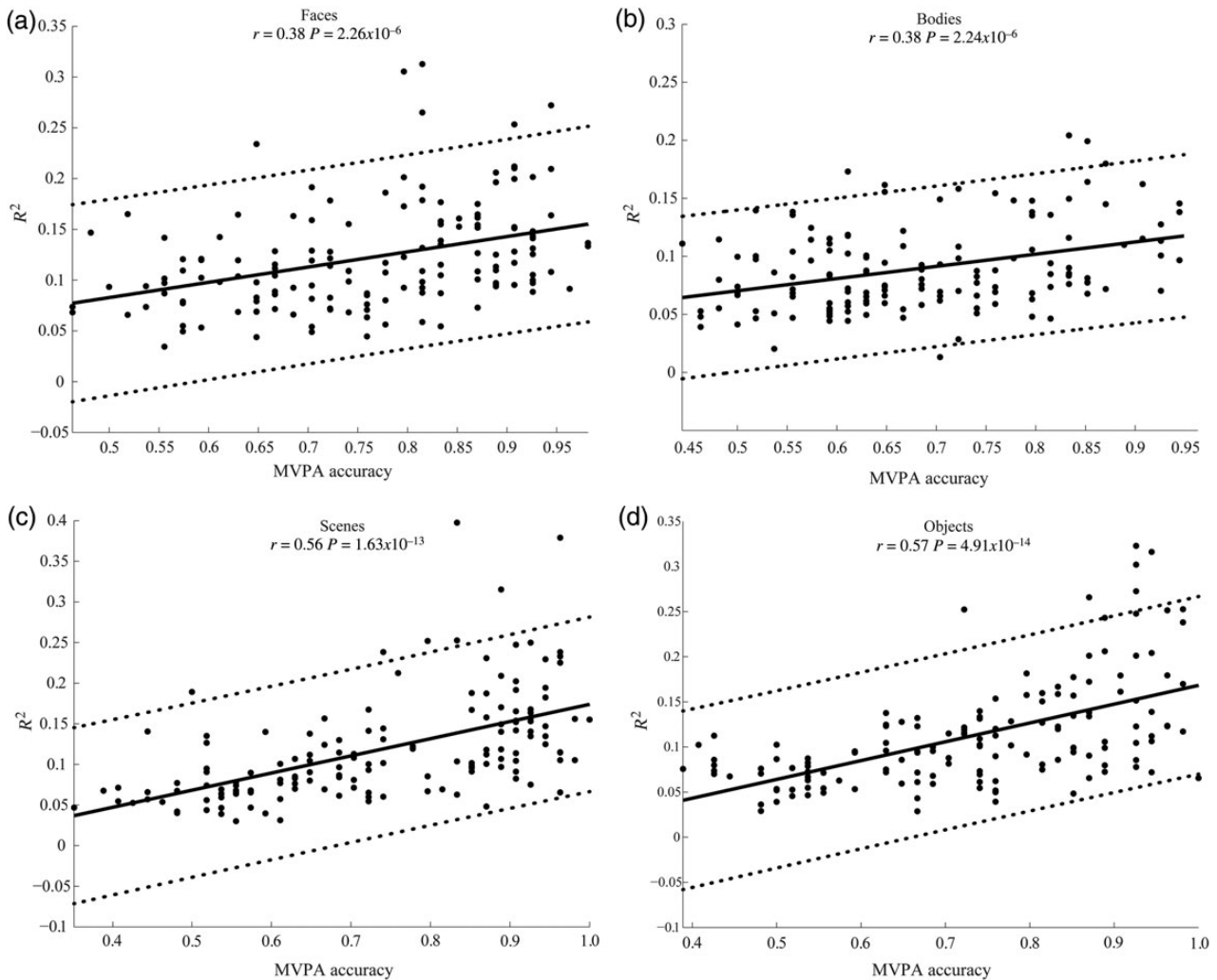


**Figure 6.** Model fits positively correlate with MVPA accuracy per anatomical parcel. The fits or  $R^2$  values for the final models of connectivity and function per anatomical region were significantly and positively correlated with MVPA accuracies to each functional contrast, which reflect the cooperative selectivity of the response patterns across voxels within each region (a) Faces, (b) Bodies, (c) Scenes, and (d) Objects. Parcels with better model fits had higher MVPA accuracy for that functional contrast.

this effect from the reliability of the functional response in a given parcel. It remains unclear whether connectivity may also fit parcels with reliable fMRI responses but low selectivity for a contrast. Future studies can model the within-subject fMRI responses (e.g., across a large number of experimental runs) for each voxel as a repeated measure, and calculate whether voxels with high selectivity (and high stability across runs) are better modeled by connectivity than voxels with lower selectivity but high stability.

### Connectivity Can Predict Neural Selectivity across a Range of Functions

These results extend prior work on face selectivity in the fusiform gyrus (Saygin et al. 2012) not only to all of cortex, but also to other high-level visual categories. Substantial evidence suggests that faces are a special perceptual category for humans and other social animals (e.g., Kanwisher 2010; McKone and Robbins 2011; Kanwisher and Dilks 2014), and so the tight relationship between connectivity and neural responses might have been restricted to face selectivity. Indeed, we found that connectivity most accurately predicted responses to faces and scenes, perhaps

reflecting the evolutionary significance of these 2 categories. Nonetheless, the neural responses for other visual categories were also accurately predicted from connectivity alone. This finding provides evidence in support of the fundamental assumption that extrinsic connections underlie brain function in general, and not only for select categories. However, the present experiment only tested high-level visual categories and whether this assumption also holds for other domains such as audition, memory, or language remains untested. Future studies can use the present approach to test the connectivity–function relationship in other domains.

Further, our results showed that connectivity was a better predictor of fMRI responses to visual categories than the only other current method for predicting voxel-wise brain function in the absence of an fMRI scan in the subject in question: a group analysis of the same functional contrast in a different set of subjects. The fact that functional predictions were more accurate from the same subject's diffusion data than from group data on the same functional contrast shows that individual connectivity was able to account for individual function. That is, connectivity was able to capture an individual's functional responses above and beyond what is common across

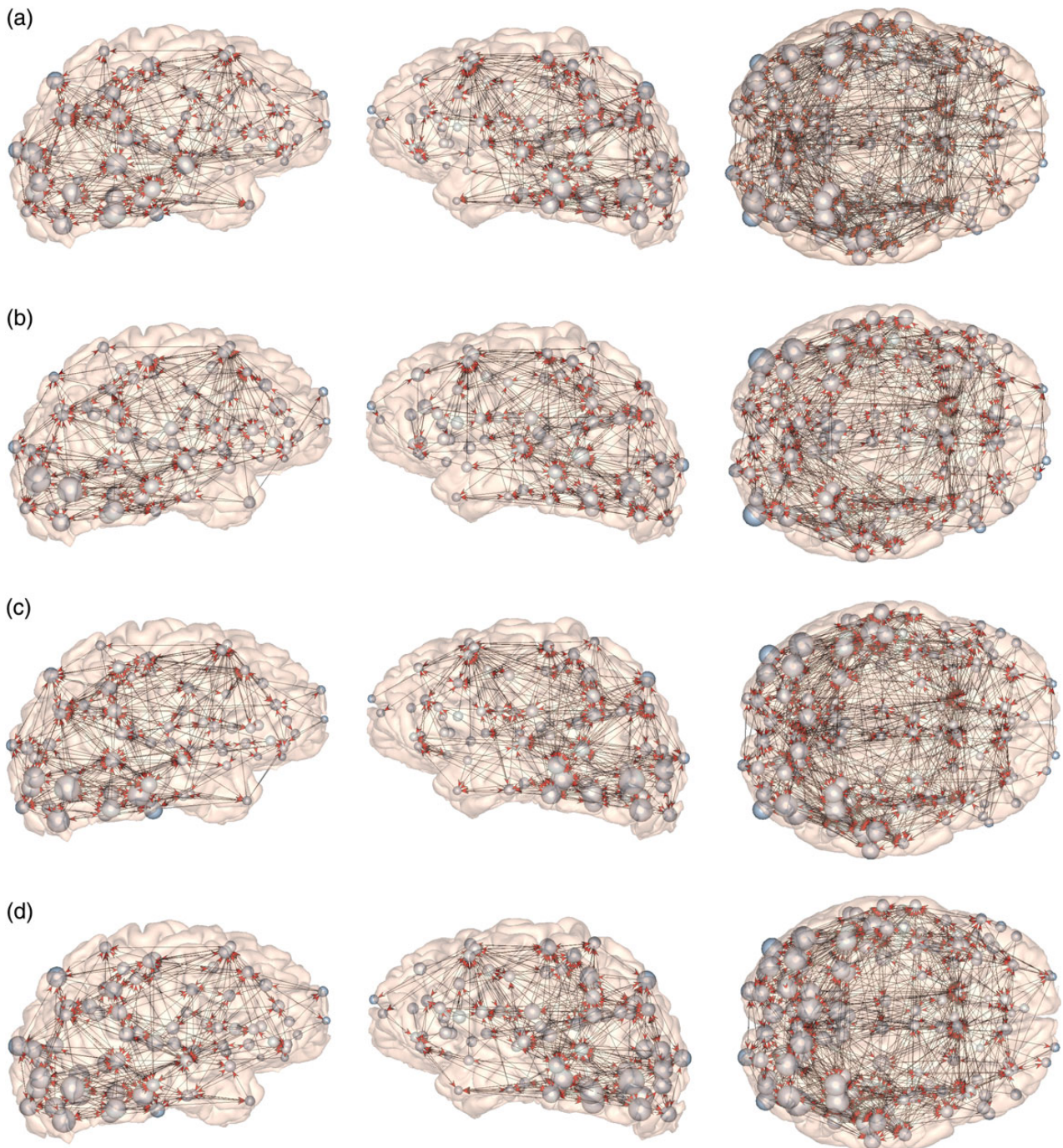


**Figure 7.** Functionally relevant networks. The functionally relevant networks (FRNs) for (a) Faces, (b) Bodies, (c) Scenes, and (d) Objects are visualized as directed graphs. Left column: right lateral surface; center column: left lateral surface; right column: ventral surface (with right hemisphere on top). In this graphical view, nodes reflect parcels, and edges are the anatomical connections that are significant predictors of neural responses. Edges originate from significant predictors, and their arrows point toward the parcels whose neural responses are predicted. For example, if node A predicts node B, then an arrow would originate from node A and point toward node B. Node size scales with selectivity, such that larger spheres represent parcels with higher selectivity.

individuals. Indeed, we found that the DWI predictions of voxel-wise functional response even had accuracy comparable with a second functional scan in the same subject on the same contrast (Supplementary Fig. 1). The use of connectivity to predict voxel-wise functional responses has substantial promise clinically, for example for determining functionally selective regions of cortex in individuals who cannot be functionally scanned (because they are comatose, unable to perform the tasks

required for functional scanning, or unable to lie still without sedation).

### Predicting Neural Function from Connectivity Reveals Functionally Relevant Networks

Among the multitude of connections within any voxel, only a subset of connections may be especially relevant to a particular

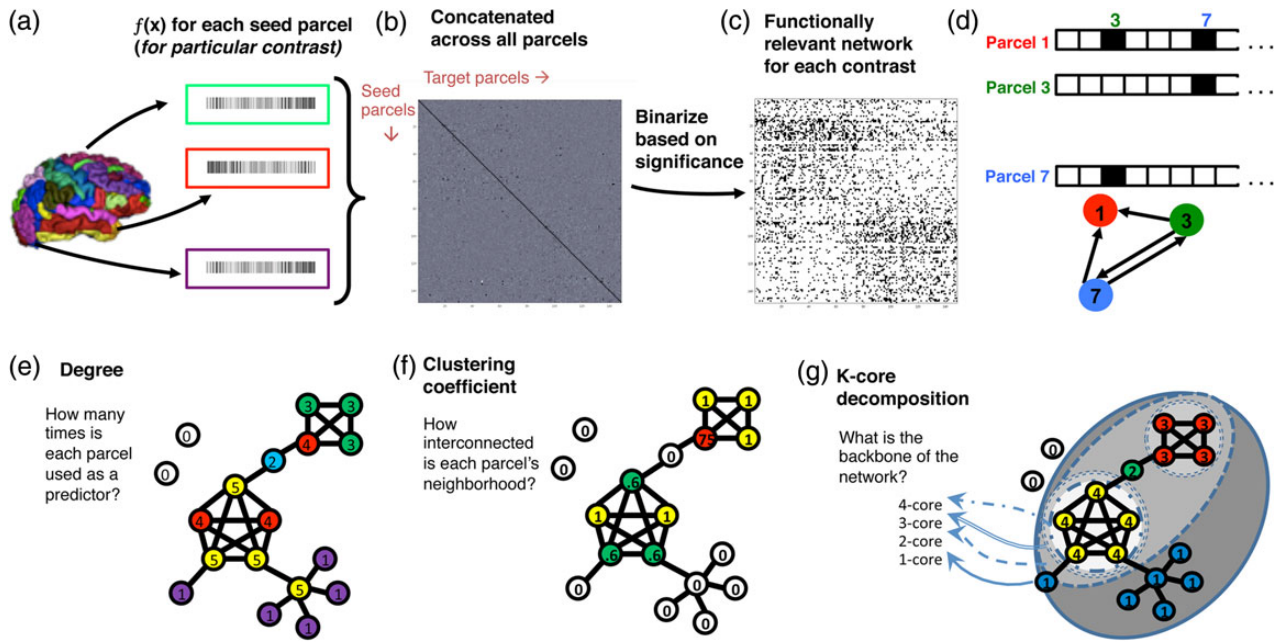


**Figure 8.** Schematic of whole-brain network analyses. (a) A final model ( $f(x)$ ) for each parcel and for each contrast is computed (see Fig. 1). (b)  $f(x)$  from all parcels are concatenated to yield a  $148 \times 148$  matrix; rows are seed parcels and columns are target parcels (predictors). This matrix is then (c) binarized based on significance (i.e., each  $f(x)$  is assigned 1 or “true” for coefficients that make a significant contribution to the model). This matrix is the functionally relevant network (FRN) for a particular fMRI contrast. Here, black squares are “true” (i.e., significant predictors) and white squares are false; the diagonal is white because a parcel cannot predict itself. (d) A closer look at a few rows of an FRN illustrates the type of information that can be gleaned about a network. For example, in the FRN for Face responses, parcels 3 and 7 predict responses in parcel 1, but parcel 1 does not predict parcels 3 and 7; instead, parcel 3’s responses are predicted by 7 and vice versa. We can represent this relationship as a directed network, with arrows pointing “from” the predictors “to” the parcels that they predict. This network diagram is used to visualize the predictor–predictee relationship for all parcels for each contrast (see Fig. 7). (e–g) We further explored this complex network using graph theory and calculated 3 metrics that reflected the role of each parcel in predicting responses in other parcels. The values for each of these metrics are shown in the nodes of a rhetorical network. (e) We calculated out-degree, which is the number of times each parcel was predictive of functional responses in every other parcel. (f) We also calculated the clustering coefficient of each parcel, which measures how interconnected the secondary network of a node is (e.g., a parcel with a high clustering coefficient would predict function in a set of other parcels, and these parcels would also predict function in one another). (g) Lastly, we calculated the core number of each parcel using k-core decomposition, which identifies the underlying backbone of a network through iterative pruning of nodes. We identified subnetworks (k-cores) by successively removing all nodes with a degree smaller than  $k$  until all remaining nodes have a degree equal to or larger than  $k$  (e.g., prune nodes with degree less than  $k$ ; if the resulting subnetwork contains nodes with degree less than  $k$ , remove them, until all nodes have degree of at least  $k$ ). Each successive k-core contains a deeper infrastructure of interconnected components. The core number of a node is the highest k-core that it belongs to.

function of interest. Indeed, it is possible that even a majority of connections are not involved in the primary function of a region. For example, <5% of the inputs to macaque primary visual cortex V1 arrive from the optic radiations (Peters et al. 1994), which are obviously critical for visual responses in V1. This consideration highlights the need to extract, out of the overwhelmingly complex connectivity patterns, the connections that most strongly influence the neural responses for a particular stimulus or behavior. We need to parse brain connectivity in a functional context in order to decipher the impact of each connection in defining a region’s functional properties (see Lee and Reid 2011; Seung 2011; Reid 2012).

The novel approach used here enables us to identify the connections that are relevant for predicting different functional selectivities, or the FRNs for each fMRI contrast. These networks offer rich information about the connections that are predictive in each parcel and for each contrast. We created directed graphs of the FRNs and analyzed them using graph theoretical metrics. Previous studies have used graph theoretical approaches to analyze structural connectivity networks; these studies commonly relate their findings to functional and/or lesion studies to better elucidate how anatomical connections support neural functions (e.g., He et al. 2007; Bullmore and Sporns 2009). In the present study, we use similar graph theoretical approaches to directly

analyze the structural networks that are predictive for each of the functional contrasts tested.

We found that the more selective a parcel is, the more frequently its connectivity predicts function in other areas (i.e., degree correlates with selectivity). Unlike functional connectivity, structural connectivity is naïve to the functional responses of the target regions; a region need not possess similar functional characteristics to be connected to (and predictive of function in) another region. Further, the connectivity models in our analyses only had information about the connection strength of the predictors, not their functional responses; it is notable that the most selective parcels were themselves predictors of function across the brain, even without any explicit modeling of the functional responses of connected regions. An alternative outcome could have been that the most selective parcels do not directly predict selectivity elsewhere, and instead share predictive information with the rest of the brain through their connections with intermediary hub nodes (such as those elucidated in Hagmann et al. 2008; Iturria-Medina et al. 2008; Gong et al. 2009). Our analyses instead show that visual categorical responses across the brain are predicted by connectivity with the most selective brain regions.

We also found that the clustering coefficient of each parcel was significantly correlated with the selectivity of the parcel for

all 4 contrasts. High clustering coefficients are commonly associated with cliques, or highly interconnected groups of nodes (Watts and Strogatz 1998). Our results suggest that the most selective parcels form cliques, in which selective parcels are both predictive “of” one another and predicted “by” one another.

Furthermore, we found significant correlations between selectivity and core number. This signifies that the most selective parcels also constitute the most foundational elements of the FRNs and that their connectivity patterns form a structural core for predicting visual selectivities throughout the brain. It is worth noting that the network metrics used to analyze the FRNs are related to one another. For example, parcels that are members of interconnected cliques may tend to have higher core numbers, and the core number of a parcel can only be as large as its degree; but while a high degree is necessary for having a high core number, it is not sufficient. Core numbers are sensitive to the overall neighborhood of each node, and depend on the features of connected nodes, as well as their own. Thus, the 3 graph theoretical metrics that we use here elucidate different features of the FRNs and the role of each parcel within that larger network. Future work may further characterize and contrast the architecture of various FRNs with more complex graphical approaches (e.g., modularity, identification of hub nodes, and overall network structure). It will also be important to expand this approach to retinotopic regions, in order to better characterize FRNs from early visual areas to higher level regions.

### Other Future Directions and Conclusions

The stimulus categories used in the present experiment represent some of the most robust and replicable perceptual domains, and thus it remains possible that the tight relationship between connectivity and function holds only for these mental functions. Connectivity may be unable to account for functional and intersubject variability in higher level processes, such as decision-making or emotional reappraisal. Testing other, particularly nonperceptual domains will be necessary to understand whether the relationship between connectivity and neural responses is a general principle of brain organization. Other future directions may include amassing a database of functional tasks and their predictability through connectivity, allowing researchers to predict the functional response to a variety of tasks within any single subject, yet requiring only the acquisition of a single-shot diffusion scan.

This approach also opens up the possibility of addressing a fundamentally important question about the developmental origins of functional specialization: does extrinsic connectivity instruct and direct the functional development of the cortex? In the current paper, we observed a tight relationship between extrinsic connectivity and function in adults, which would be expected if pre-existing connectivity fingerprints play a causal role in subsequent development of functional specialization. Researchers will not only be able to use this novel method to study the differentiation of connectivity patterns across the cortex in early development, but also ascertain whether connectivity patterns early in life determine subsequent differentiation of function.

The current results open a window into the coupling between the structural organization of the brain and its functional specialization. Other anatomical factors, such as intrinsic connectivity or cytoarchitecture, undoubtedly play a key role in determining the functional responses of a region. Recent work suggests that cortical folding patterns and other macroanatomical landmarks may also allow trained observers to locate high-level visual

regions (Grill-Spector and Weiner 2014; Weiner et al. 2014). Future studies can combine connectivity information with macroanatomical landmarks to generate individual subject predictions, and evaluate the contribution of these various anatomical factors in predicting function. Our analyses nonetheless revealed that, in the absence of any other information, the input-output relations of a region (i.e., its extrinsic connections) may be used to accurately predict functional clusters that are variable across the population. And although we cannot distinguish between input and output with DWI, the present findings demonstrate that functionally specialized cortical regions send and receive specialized projections for category-selective visual function at a fine spatial grain across the human cortex.

### Supplementary Material

Supplementary material can be found at: <http://www.cercor.oxfordjournals.org/>.

### Authors' Contributions

D.E.O. and Z.M.S. designed and performed experiments, analyzed data, and wrote the manuscript. K.K. designed and performed experiments. J.D.E.G., N.K., and R.R.S. designed experiments and wrote the manuscript.

### Funding

This work was supported by funds from the NICHD/NIH grant F32HD079169, McGovern Institute Neurotechnology fellowship, T32 MH081728, T32 EY013935, Ellison Medical Foundation, and the Simons Foundation and Simons Center for the Social Brain at MIT.

### Notes

We thank the Athinoula A. Martinos Imaging Center at the McGovern Institute for Brain Research at MIT, and the study participants and their families, including those participating in the SFARI Simplex Collection and the Autism Consortium, as well as the principle investigators at SFARI SSC sites.

### References

- Alvarez-Hamelin JI, Dall'Asta L, Barrat A, Vespignani A. 2005. Large scale networks fingerprinting and visualization using the k-core decomposition. In: Weiss Y, Scholkopf B, Platt J, editors. *Advances in neural information processing systems*. Cambridge (Massachusetts): MIT Press. p. 41–50.
- Beckmann M, Johansen-Berg H, Rushworth MFS. 2009. Connectivity-based parcellation of human cingulate cortex and its relation to functional specialization. *J Neurosci*. 29:1175–1190.
- Behrens TEJ, Berg HJ, Jbabdi S, Rushworth MFS, Woolrich MW. 2007. Probabilistic diffusion tractography with multiple fibre orientations: what can we gain? *Neuroimage*. 34:144–155.
- Bock DD, Lee W-CA, Kerlin AM, Andermann ML, Hood G, Wetzel AW, Yurgenson S, Soucy ER, Kim HS, Reid RC. 2011. Network anatomy and in vivo physiology of visual cortical neurons. *Nature*. 471:177–182.
- Briggman KL, Helmstaedter M, Denk W. 2011. Wiring specificity in the direction-selectivity circuit of the retina. *Nature*. 471: 183–188.

- Bullmore E, Sporns O. 2009. Complex brain networks: graph theoretical analysis of structural and functional systems. *Nat Rev Neurosci*. 10:186–198.
- Colby CL, Goldberg ME. 1999. Space and attention in parietal cortex. *Annu Rev Neurosci*. 22:319–349.
- Desimone R, Albright TD, Gross CG, Bruce C. 1984. Stimulus-selective properties of inferior temporal neurons in the macaque. *J Neurosci*. 4:2051–2062.
- Destrieux C, Fischl B, Dale A, Hagren E. 2010. Automatic parcellation of human cortical gyri and sulci using standard anatomical nomenclature. *Neuroimage*. 53:1–15.
- Fedorenko E, Hsieh P-J, Nieto-Castañón A, Whitfield-Gabrieli S, Kanwisher N. 2010. New method for fMRI investigations of language: defining ROIs functionally in individual subjects. *J Neurophysiol*. 104:1177–1194.
- Felleman DJ, Van Essen DC. 1991. Distributed hierarchical processing in the primate cerebral cortex. *Cereb Cortex*. 1:1–47.
- Fischl B, Salat DH, Busa E, Albert M, Dieterich M, Haselgrove C, van der Kouwe A, Killiany R, Kennedy D, Klaveness S, et al. 2002. Whole brain segmentation. *Neuron*. 33:341–355.
- Fischl B, van der Kouwe A, Destrieux C, Hagren E, Ségonne F, Salat DH, Busa E, Seidman LJ, Goldstein J, Kennedy D, et al. 2004. Automatically parcellating the human cerebral cortex. *Cereb Cortex*. 14:11–22.
- Freiwald WA, Tsao DY. 2014. Neurons that keep a straight face. *Proc Natl Acad Sci USA*. 111:7894–7895.
- Frost MA, Goebel R. 2012. Measuring structural-functional correspondence: spatial variability of specialised brain regions after macro-anatomical alignment. *Neuroimage*. 59:1369–1381.
- Glickfeld LL, Andermann ML, Bonin V, Reid RC. 2013. Cortico-cortical projections in mouse visual cortex are functionally target specific. *Nat Neurosci*. 16:219–226.
- Gong G, He Y, Concha L, Lebel C, Gross DW, Evans AC, Beaulieu C. 2009. Mapping anatomical connectivity patterns of human cerebral cortex using in vivo diffusion tensor imaging tractography. *Cereb Cortex*. 19:524–536.
- Grill-Spector K, Weiner KS. 2014. The functional architecture of the ventral temporal cortex and its role in categorization. *Nat Rev Neurosci*. 15:536–548.
- Hagmann P, Cammoun L, Gigandet X, Meuli R, Honey CJ, Wedeen VJ, Sporns O. 2008. Mapping the structural core of human cerebral cortex. *PLoS Biol*. 6:e159.
- Hastie T, Tibshirani R, Friedman J. 2009. The elements of statistical learning: data mining, inference, and prediction. 2nd edition. New York: Springer.
- Haxby JV, Gobbini MI, Furey ML, Ishai A, Schouten JL, Pietrini P. 2001. Distributed and overlapping representations of faces and objects in ventral temporal cortex. *Sci*. 293:2425–2430.
- He BJ, Snyder AZ, Vincent JL, Epstein A, Shulman GL, Corbetta M. 2007. Breakdown of functional connectivity in frontoparietal networks underlies behavioral deficits in spatial neglect. *Neuron*. 53:905–918.
- Iturria-Medina Y, Sotero RC, Canales-Rodríguez EJ, Alemán-Gómez Y, Melie-García L. 2008. Studying the human brain anatomical network via diffusion-weighted MRI and Graph Theory. *Neuroimage*. 40:1064–1076.
- Jbabdi S, Behrens TE. 2013. Long-range connectomics. *Ann N Y Acad Sci*. 1305:83–93.
- Jbabdi S, Lehman JF, Haber SN, Behrens TE. 2013. Human and monkey ventral prefrontal fibers use the same organizational principles to reach their targets: tracing versus tractography. *J Neurosci*. 33:3190–3201.
- Jbabdi S, Sotiropoulos SN, Behrens TE. 2013. The topographic connectome. *Curr Opin Neurobiol*. 23:207–215.
- Johansen-Berg H, Behrens TEJ, Robson MD, Drobnjak I, Rushworth MFS, Brady JM, Smith SM, Higham DJ, Matthews PM. 2004. Changes in connectivity profiles define functionally distinct regions in human medial frontal cortex. *Proc Natl Acad Sci USA*. 101:13335–13340.
- Julian JB, Fedorenko E, Webster J, Kanwisher N. 2012. An algorithmic method for functionally defining regions of interest in the ventral visual pathway. *Neuroimage*. 60:2357–2364.
- Kanwisher N. 2010. Functional specificity in the human brain: a window into the functional architecture of the mind. *Proc Natl Acad Sci USA*. 107:11163–11170.
- Kanwisher N, Dilks DD. 2014. The functional organization of the ventral visual pathway in humans. In: Werner JS, Chalupa LM, editors. *The new visual neurosciences*. Cambridge: MIT Press. p. 733–748.
- Kanwisher N, McDermott J, Chun MM. 1997. The fusiform face area: a module in human extrastriate cortex specialized for face perception. *J Neurosci*. 17:4302–4311.
- Lee W-CA, Reid RC. 2011. Specificity and randomness: structure-function relationships in neural circuits. *Curr Opin Neurobiol*. 21:801–807.
- Lick DR, White AT. 1970. k-Degenerate graphs. *Can J Math*. 22:1082–1096.
- Mars RB, Jbabdi S, Sallet J, O'Reilly JX, Croxson PL, Olivier E, Noonan MP, Bergmann C, Mitchell AS, Baxter MG. 2011. Diffusion-weighted imaging tractography-based parcellation of the human parietal cortex and comparison with human and macaque resting-state functional connectivity. *J Neurosci*. 31:4087–4100.
- Mars RB, Sallet J, Neubert F-X, Rushworth MFS. 2013. Connectivity profiles reveal the relationship between brain areas for social cognition in human and monkey temporoparietal cortex. *Proc Natl Acad Sci*. 110:10806–10811.
- Mars RB, Sallet J, Schüffelgen U, Jbabdi S, Toni I, Rushworth MFS. 2012. Connectivity-based subdivisions of the human right “temporoparietal junction area”: evidence for different areas participating in different cortical networks. *Cereb Cortex*. 22:1894–1903.
- McCarthy G, Puce A, Gore JC, Allison T. 1997. Face-specific processing in the human fusiform gyrus. *J Cogn Neurosci*. 9:605–610.
- McKone E, Robbins R. 2011. Are faces special. In: *Oxford handbook of face perception*. UK: Oxford University Press Oxford. p. 149–176.
- Moeller S, Freiwald WA, Tsao DY. 2008. Patches with links: a unified system for processing faces in the macaque temporal lobe. *Sci*. 320:1355–1359.
- Passingham RE, Stephan KE, Kotter R. 2002. The anatomical basis of functional localization in the cortex. *Nat Rev Neurosci*. 3:606–616.
- Perrett DI, Hietanen JK, Oram MW, Benson PJ, Rolls ET. 1992. Organization and functions of cells responsive to faces in the temporal cortex [and Discussion]. *Philos Trans R Soc London Ser B Biol Sci*. 335:23–30.
- Peters A, Payne BR, Budd J. 1994. A numerical analysis of the geniculocortical input to striate cortex in the monkey. *Cereb Cortex*. 4:215–229.
- Pitcher D, Dilks DD, Saxe RR, Triantafyllou C, Kanwisher N. 2011. Differential selectivity for dynamic versus static information in face-selective cortical regions. *Neuroimage*. 56:2356–2363.
- Postelnicu G, Zollei L, Fischl B. 2009. Combined volumetric and surface registration. *IEEE Trans Med Imaging*. 28:508–522.
- Reese TG, Heid O, Weisskoff RM, Wedeen VJ. 2003. Reduction of eddy-current-induced distortion in diffusion MRI using a twice-refocused spin echo. *Magn Reson Med*. 49:177–182.

- Reid RC. 2012. From functional architecture to functional connectomics. *Neuron*. 75:209–217.
- Rosa-Salva O, Regolin L, Vallortigara G. 2010. Faces are special for newly hatched chicks: evidence for inborn domain-specific mechanisms underlying spontaneous preferences for face-like stimuli. *Dev Sci*. 13:565–577.
- Sallet J, Mars RB, Noonan MP, Neubert F-X, Jbabdi S, O'Reilly JX, Filippini N, Thomas AG, Rushworth MF. 2013. The organization of dorsal frontal cortex in humans and macaques. *J Neurosci*. 33:12255–12274.
- Saxe R, Brett M, Kanwisher N. 2006. Divide and conquer: a defense of functional localizers. *Neuroimage*. 30:1088–1096. discussion 1097. –9.
- Saygin ZM, Osher DE, Augustinack J, Fischl B, Gabrieli JDE. 2011. Connectivity-based segmentation of human amygdala nuclei using probabilistic tractography. *Neuroimage*. 56:1353–1361.
- Saygin ZM, Osher DE, Koldewyn K, Reynolds G, Gabrieli JDE, Saxe RR. 2012. Anatomical connectivity patterns predict face selectivity in the fusiform gyrus. *Nat Neurosci*. 15:321–327.
- Seidman SB. 1983. Network structure and minimum degree. *Soc Netw*. 5:269–287.
- Seung HS. 2011. Neuroscience: towards functional connectomics. *Nature*. 471:170–172.
- Sewards TV. 2011. Neural structures and mechanisms involved in scene recognition: a review and interpretation. *Neuropsychologia*. 49:277–298.
- Sugita Y. 2008. Face perception in monkeys reared with no exposure to faces. *Proc Natl Acad Sci USA*. 105:394–398.
- Sur M, Garraghty PE, Roe AW. 1988. Experimentally induced visual projections into auditory thalamus and cortex. *Science*. 242:1437–1441.
- Tomassini V, Jbabdi S, Klein JC, Behrens TEJ, Pozzilli C, Matthews PM, Rushworth MFS, Johansen-Berg H. 2007. Diffusion-weighted imaging tractography-based parcellation of the human lateral premotor cortex identifies dorsal and ventral subregions with anatomical and functional specializations. *J Neurosci*. 27:10259–10269.
- Tsao DY, Freiwald WA, Tootell RBH, Livingstone MS. 2006. A cortical region consisting entirely of face-selective cells. *Science*. 311:670–674.
- Turati C, Bulf H, Simion F. 2008. Newborns' face recognition over changes in viewpoint. *Cognition*. 106:1300–1321.
- Ungerleider LG, Mishkin M. 1982. Two cortical visual systems. In: Ingle D, Goodale MA, Mansfield RJW, editors. *Analysis of visual behaviour*. Cambridge: MIT Press. p. 549–586.
- Warrington EK, James M. 1967. An experimental investigation of facial recognition in patients with unilateral cerebral lesions. *Cortex*. 3:317–326.
- Watts DJ, Strogatz SH. 1998. Collective dynamics of “small-world” networks. *Nature*. 393:440–442.
- Weiner KS, Golarai G, Caspers J, Chuapoco MR, Mohlberg H, Zilles K, Amunts K, Grill-Spector K. 2014. The mid-fusiform sulcus: a landmark identifying both cytoarchitectonic and functional divisions of human ventral temporal cortex. *Neuroimage*. 84:453–465.
- Zöllei L, Stevens A, Huber K, Kakunoori S, Fischl B. 2010. Improved tractography alignment using combined volumetric and surface registration. *Neuroimage*. 51:206–213.